analytical chemistry

pubs.acs.org/ac Article

Combining Fourier Transform Ion Mobility with Charge Detection Mass Spectrometry for the Analysis of Multimeric Protein Complexes

Kyle J. Juetten, James D. Sanders, Michael T. Marty, and Jennifer S. Brodbelt*

Cite This: *Anal. Chem.* 2025, 97, 140−146 Read Online

ACCESS | Metrics & More | Article Recommendations | Supporting Information

ABSTRACT: Charge detection mass spectrometry (CDMS) allows direct mass measurement of heterogeneous samples by simultaneously determining the charge state and the mass-to-charge ratio (m/z) of individual ions, unlike conventional MS methods that use large ensembles of ions. CDMS typically requires long acquisition times and the collection of thousands of spectra, each containing tens to hundreds of ions, to generate sufficient ion statistics, making it difficult to interface with the time scales of online separation techniques such as ion mobility. Here, we demonstrate the application of Fourier transform multiplexing and drift tube ion mobility joined with Orbitrap-based CDMS for the analysis of multimeric protein complexes. Stepped frequency modulation was utilized to enable unambiguous frequency assignment during mobility sweeps and allow spectral averaging, which improves the accuracy and signal-to-noise of ion mobility spectra and CDMS measurements. Fourier transformation of the signal reveals the arrival times and collision cross sections of ions while simultaneously collecting charge information for thousands of individual ions. Combining Fourier transform multiplexing ion mobility and CDMS provides insight into each ion's size and mass while showcasing a potential solution to the duty cycle mismatch of online separation techniques in the single ion regime.

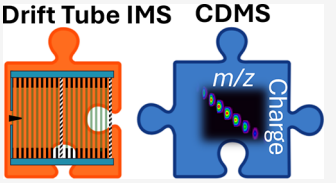

INTRODUCTION

Assignment of mass-to-charge (m/z) in mass spectrometry depends on separation of charge states and/or isotopic resolution. During electrospray ionization mass spectrometry, ions are typically produced in an array of charge states, which can be used to calculate their charge and mass.[1] This charge state/mass inference process becomes more difficult for large macromolecular complexes owing to their large isotopic envelopes, heterogeneity of post-translational modifications, salt/solvent adducts, and sequence variants, which complicate mass spectra and impede the ability to resolve and assign charge states.[2] Charge detection mass spectrometry (CDMS) overcomes this hurdle by measuring an analyte's charge directly along with its m/z ratio.[3,4] Many of the previous advances in CDMS were accomplished on custom-built electrostatic linear ion trap instruments that facilitated near perfect charge assignment.[5−11] More recently, CDMS has been adapted for Orbitrap mass spectrometers, making the concept of charge-based detection more widely accessible on commercial instruments.[12−15]

A typical ensemble mass spectrum is the result of simultaneously analyzing many thousands of ions, whereas a spectrum acquired by CDMS lies in the single particle regime. In this regime, the measured signal is directly proportional to the total charge of the particle, allowing direct charge measurement.[16] This CDMS strategy has facilitated the analysis of megadalton-sized ions, such as adeno-associated viruses (AAVs) and ribosomes, that would be near impossible by traditional MS methods.[7,11,13,16−22] Charge detection also boosts the sensitivity of mass spectrometry experiments because sample concentrations in the nanomolar to picomolar range are needed for individual ion measurements rather than the typical micromolar range for ensemble measurements.[16,23]

The impact of CDMS can be further expanded by integration with online separation techniques. This union presents some inherent challenges given the lengthy collection times required for CDMS data. Typically, hundreds or thousands of spectra are collected for CDMS experiments to ensure sufficient signal-to-noise of mass measurements, an experimental demand that creates an inherent mismatch with online separation techniques such as liquid chromatography or capillary electrophoresis, which allow only a few hundred scans per elution band. Some recent reports have showcased the challenge of aligning separation methods with CDMS. For example, nanoflow liquid chromatography was interfaced with Orbitrap-based charge detection for the analysis of the proteins transferrin and β-galactosidase as well as the glycoproteins etanercept and α-1-acid glycoprotein.[24] It was noted that many CDMS spectra exhibited low signal-to-noise compared to mass spectra obtained by standard infusion experiments.[24] Another study showcased a comparison of the number of ions collected

Received: July 1, 2024
Revised: December 2, 2024
Accepted: December 24, 2024
Published: December 30, 2024

https://doi.org/10.1021/acs.analchem.4c03379
Anal. Chem. 2025, 97, 140−146

as well as the quality of mass assignment for varying elution profiles via capillary electrophoresis CDMS and found that shorter elution profiles produced lower quality data.[25] One recent study examined the elution profiles of antibodies introduced by an online buffer exchange method coupled with CDMS.[26] These studies confirm that the duty cycle mismatch requires compromises, usually in the CDMS data quality. Most recently, CDMS was coupled with size exclusion chromatography via a Hadamard transform multiplexing strategy that allowed multiple injections to be stacked to increase the duty cycle.[27]

The challenges of integrating CDMS with a gas-phase separation method like drift tube ion mobility are even more daunting as the rapid migration times of ions are incompatible with the transient lengths required for Orbitrap-based CDMS measurements. This duty cycle mismatch between drift tube ion mobility and Orbitrap mass analysis has been addressed previously using Fourier transform multiplexing, where ion drift times are encoded through the modulation of the ion gates.[28−32] During acquisition of mass spectra, ion gates are opened and closed simultaneously at a gradually increasing frequency. This encodes ion drift times as a pattern of signal oscillations, which can then be Fourier transformed to generate a frequency spectrum that is subsequently converted to an arrival time distribution. To marry this technique with CDMS, stepped frequency modulation must be employed to ensure unambiguous frequency designation as well as allow the collection of multiple CDMS scans at each frequency. This allows ions from multiple scans to be binned, improving the signal-to-noise of CDMS data.[33,34]

Herein, we have interfaced multiplexed drift tube ion mobility with CDMS for the analysis of multimeric protein complexes: alcohol dehydrogenase, glutamate dehydrogenase, GroEL, and etanercept. Coupling CDMS with ion mobility offers the potential for measurements of CCS for sample- or signal-limited applications not possible with conventional ion mobility mass spectrometry. The present method uses a home-built drift tube and Python code to designate frequency sweeps needed for ion mobility experiments. Additionally, modifications were made to the open-source UniDec software platform to enable the processing of multiplexed CDMS data. These modifications combined with Orbitrap-based CDMS allow high accuracy and precision mass assignment of macromolecules while also providing structural information about native protein complexes.

EXPERIMENTAL SECTION

Materials. Alcohol dehydrogenase (ADH) from yeast and glutamate dehydrogenase (GDH) from bovine liver were purchased from Millipore Sigma. GroEL was purified as previously described.[35] Etanercept was obtained from Myoderm (Norristown, PA). Samples were buffer-exchanged into 100 mM ammonium acetate using Micro Bio-Spin P6 spin columns (BioRad, Hercules, CA) per manufacturer's instructions and diluted to final protein concentrations of 1 μM. This protein concentration is higher than used in conventional CDMS experiments (∼1 to 10 nM) owing to the low transmission efficiency of the atmospheric pressure drift tube. All samples were run in triplicate. Ion mobility spectra are from a single representative replicate.

Instrumentation. The atmospheric pressure drift tube was constructed from printed circuit board electrodes and uses a ∼10 cm desolvation region and a ∼10 cm drift region along with two ion gates for FT multiplexing as described previously.[36] A voltage is applied across the resistor chain to create a uniform electric field. Drift voltages of 4, 6, 8, and 10 kV were used corresponding to electric field strengths of 200, 300, 400, and 500 V/cm. The ion gates are controlled by supplying a voltage of 75 V (front) or 85 V (back) above the standard potential at their respective locations using a pair of FET pulsers built by GAA Custom Engineering (Kennewick, WA). Frequency sweeps were generated by custom Python scripts and covered a frequency range from 5 to 505 Hz. Gating waveforms were applied using an Arduino-compatible microcontroller (Wio Terminal, Seeedstudio) and synchronized with the scans of the mass spectrometer by using the split lens signal output as a trigger, as described previously.[33] Additionally, a voltage level shifter was utilized to accommodate the different signal levels from the mass spectrometer and Arduino microcontroller. A schematic of this configuration is shown in Figure 1. FT multiplexed acquisition using the

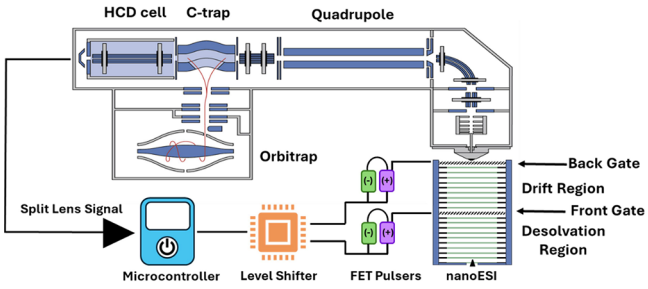

Figure 1. Schematic of the Thermo Scientific Q Exactive Plus UHMR Orbitrap mass spectrometer equipped with an atmospheric pressure drift tube for IM-CDMS experiments. Drift tube has two ion gates which are controlled by a set of open-source ion gate pulsers to enable FT multiplexing. Frequency changes are synchronized with mass scans by connecting the pulsers to the split lens signal output from the mass spectrometer.

atmospheric drift tube is performed by opening and closing both back and front gates simultaneously at gradually increasing frequency using a symmetric square waveform. This frequency-gradient gating method encodes ion drift times as oscillations in the recorded ion current. As the frequency range is swept, ions with varying drift times are transmitted, while others are transmitted at minimum intensity, creating a periodic oscillating signal over the course of the sweep. This periodic signal is then Fourier transformed to generate a frequency spectrum, which in turn is converted to an arrival time distribution (ATD) by dividing the frequency vector by the sweep rate used in the acquisition. The ATDs can then be converted into ion mobility spectra using the Mason-Schamp equation (see additional details in Supporting Information; eqs S1, S2).

The drift tube was coupled to a Thermo Scientific Q Exactive Plus UHMR Orbitrap mass spectrometer (Bremen, Germany) with direct mass technology (DMT) mode enabled for all MS analysis. Samples were infused by nanoelectrospray ionization using gold/palladium-coated borosilicate emitters (20 nm i.d.) pulled in-house. A spray voltage of 1.1−1.3 kV was applied. To achieve the appropriate number of ions, a manual injection time was set (typically ∼100 to 200 ms) so that a dense spectrum (i.e., containing many different types of ions) was generated at the start of the experiments while minimizing double/triple ions, the latter which confound

https://doi.org/10.1021/acs.analchem.4c03379
Anal. Chem. 2025, 97, 140−146

charge assignment. Using a manual injection time allows attenuation of the ion current to the single ion regime and minimizes double and triple ion events. Mass spectra were collected at a resolution of 100,000 at m/z 400 for all experiments. A variety of higher-energy collisional dissociation (HCD) energies, in-source trapping, and trapping gas pressures were used for each protein analyzed, and a more detailed description of parameters is provided in Table S1.

Data Processing. When the DMT option is enabled on the UHMR mass spectrometer, the instrument stores additional transient information in the.RAW files that can be directly read and processed by STORIboard (Proteinaceous) to convert the files into a.DMT format. The voting v3 algorithm was used for charge assignment, and the parameters used are as follows: bin size of 1.5 ppm, minimum ions in each bin set to 1, number of charge neighbors set to 2, and number of isotope neighbors set to 10. A more detailed description of STORI processing parameters is given in Table S2. Processed.DMT files were then imported into UniChromCD for processing of ion mobility data. Data was processed using a m/z and mass bin size of 10. Spectral averaging of 5−15 was used depending on the experimental parameters. The STORI slopes were converted using a calibration curve generated from direct infusion experiments of ADH, GDH, and GroEL and were plotted in UniDecCD (Figure S1). Ion mobility data were demultiplexed using both magnitude and absorption mode Fourier transforms for comparison. Extracted drift times are converted into collision cross sections (CCS) using the Mason-Schamp equation.[37] All parameters used to determine the CCS values are included in Supporting Information. The fwhm was calculated using Python functions. A more detailed description of the demultiplexing algorithm implemented is provided elsewhere.[38] The compiled UniDec program and source code is provided at: https://github.com/michaelmarty/UniDec.

RESULTS AND DISCUSSION

Comparison of Ion Mobility Parameters. Evaluation and optimization of key ion mobility (IM) parameters is pivotal for successful separation and conformational analysis of multimeric protein complexes by IM-CDMS. This optimization was undertaken for the hexameric GDH complex (~337 kDa) as a suitable benchmark for developing a framework applicable to other even larger proteins of interest. Key parameters examined included the applied drift voltage, frequency step size, and the number of scans collected at each frequency, referred to as repeats. These parameters significantly influence the performance and resolution of the drift tube for multiplexed ion mobility for CDMS measurements. Examples of replicates of ion mobility spectra are shown in Figure S2 for GDH (32+) for one set of ion mobility parameters, yielding a relative standard deviation of 1.8% for the full width at half-maximum (fwhm) of the dominant feature.

The drift voltage is another parameter that impacts the speed at which ions traverse the drift tube. Applying higher drift voltages increases mobility resolution, albeit at the cost of increased collision energy, which can potentially disrupt gas-phase structure and broaden the ion mobility spectra.[39] We evaluated the impact of drift voltages of 4, 6, 8, and 10 kV by monitoring the fwhm of the dominant feature in the mobility spectrum for the representative 32+ charge state of GDH (Figure 2). The mobility spectra produced by each drift

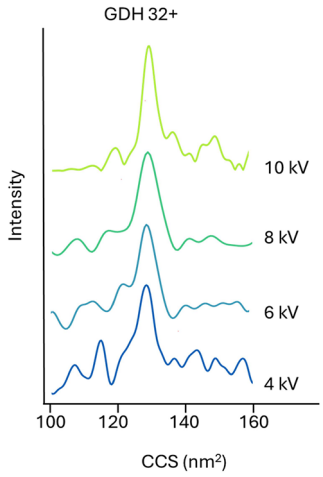

Figure 2. Comparison of the impact of drift voltages on the mobility spectra for the 32+ charge state (corresponding to (m/z 10534) of glutamate dehydrogenase (337 kDa) collected using a fixed step-size of 3 Hz and 15 repeats.

voltage were of similar quality based on visual assessment of S/N, with the 10 kV setting yielding a slightly more narrow peak width for the most prominent feature in the mobility spectrum, averaging a fwhm of 8.6 nm^2. Comparatively, the fwhm's for 4, 6, and 8 kV were 9.6, 9.1, and 10.9 nm^2, respectively. Considering the level of noise in the ion mobility spectra, the change in mobility resolution is not considered significant.

Next, the appropriate frequency step size was determined. The frequency step size determines how many frequencies are sampled throughout the experiment. For instance, a step size of 3 Hz with a frequency sweep from 5 to 505 Hz translates to data collection points at 5, 8, 11 Hz, and so forth for a total of 167 data collection points. A smaller step size enhances the sampling rate and the number of points in the resulting mobility spectrum at the expense of longer data acquisition times. The impact of collecting a lower number of points in the mobility spectrum can be partially mitigated by zero-padding to artificially increase the number of sample points and smooth features in the underlying spectrum. We evaluated step sizes of 3, 4, and 5 Hz using a fixed drift voltage of 10 kV and 15 repeats (Figure 3). The fwhm of the dominant peak in the

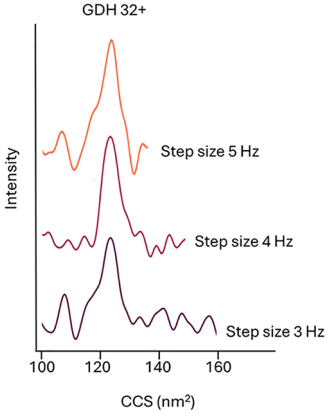

Figure 3. Impact of frequency step size on the mobility spectra for the 32+ charge state (corresponding to m/z 10534) of glutamate dehydrogenase using a drift voltage of 10 kV and 15 repeats. Larger step sizes result in collection of fewer data points.

https://doi.org/10.1021/acs.analchem.4c03379
Anal. Chem. 2025, 97, 140−146

mobility spectra acquired using these step sizes were 9.8, 10.0, and 10.2 nm^2, respectively, for the 32+ charge state of GDH. Although these values are nominally comparable, a key consideration is the final point in the mobility spectrum, defined by the maximum sweep frequency divided by the step size. A step size of 5 Hz resulted in a final data collection point corresponding to a collision cross section (CCS) of 138 nm^2, which is close to the CCS of GDH. Thus, step sizes larger than 5 Hz would fail to capture the CCS accurately. Based on these results, using any step size less than 5 Hz is suitable, with 3 Hz chosen for the remainder of the study owing to the longer total experiment time which facilitates the interrogation of more ions. All step sizes yielded nearly identical CCS values for GDH.

The number of repeats acquired at each frequency, analogous to the number of averages, is another crucial parameter that determines the total number of scans and consequently the number of ions analyzed during the experiment. During data processing these repeat scans are grouped together to allow acquisition of multiple CDMS scans at each frequency point. We evaluated repeats of 5, 10, and 15, and the mobility spectra are shown in Figure 4. The resulting

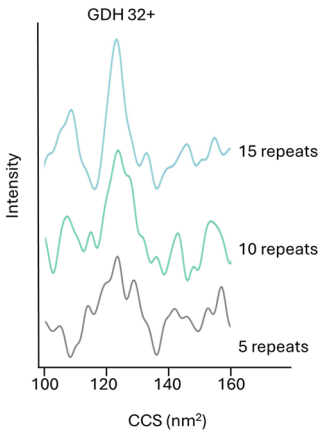

Figure 4. Influence of number of repeats on the mobility spectra for the 32+ charge state (corresponding to m/z 10,534) of GDH using a drift voltage of 10 kV and 3 Hz step size. Higher repeat numbers result in smoother mobility spectra and the collection of more ions.

CCS for the 32+ charge state of GDH was consistent across all tested parameters, but the number of ions collected and the quality of the mobility spectra varied significantly (Figure 4). The processed ion counts averaged 7242, 11,654, and 20,781 for 5, 10, and 15 repeats, respectively. Higher ion counts corresponded with smoother mobility spectra, although all repeat values produced similar peak intensity values. This outcome is sensible as the scan-to-scan variability in CDMS experiments can be quite high, so increasing the acquisition length by averaging more repeats improves data quality. This parameter also has a small, but notable impact on the mass domain data (Figure S3). Increasing the number of repeats results in a smoother mass distribution with reduced baseline noise. While a repeat number of 5 still provided accurate information about the mass of the protein, 15 repeats were selected for all subsequent experiments, due to the observed improvements in mobility data quality and the increased ion counts.

Finally, it is important to discuss the data processing techniques used to generate the mobility spectra. The data processing here utilizes the absorption mode Fourier transform, which only uses the real portion of the Fourier transform and has been previously established.[28] This contrasts with more traditional Fourier transforms (or magnitude mode), which use both the real and imaginary portions. Employing the absorption FT mode may increase mobility resolution compared to the magnitude FT mode (Figure S4) (as reported in a previous study[28]), but the emergence of new features in the mobility profile are yet unexplained. Additional details regarding the data processing techniques used in the present work are described elsewhere.[38]

Results for Protein Complexes. The integrated IM-CDMS strategy was applied to analyze multimeric protein complexes including GDH, ADH, and GroEL. We evaluated the reproducibility of the method, compared CCS values (reported here based on the value at the maximum intensity of the mobility spectrum) to previously published results, and assessed accuracies of the mass measurements. For the GDH complex, charge states from 27+ to 33+ were observed. However, CCS information was only obtainable for the 28+ to 33+ charge states, as the signal from the lowest charge state (27+) was too sparse to collect reliable data. GDH displayed CCS values ranging from 117 nm^2 (28+) to 127 nm^2 (35+) for the analyzed charge states (Figure 5), generally consistent with published values that ranged from 127 nm^2 (31+)[40,41] to 128 nm^2 (37+)[40−42] and demonstrating relative standard deviations (RSDs) below 1% for all charge states analyzed. Additional comparisons of our experimental CCS values to ones previously reported are included in Table S3 for GDH. As expected, the CCS increased slightly with the charge state of the ion, indicative of minor unfolding or elongation. Most of the mobility spectra were generally symmetric, although the 34+ and 35+ charge states exhibited small shoulders and all of the mobility spectra displayed other minor features, which could represent unresolved conformational features or may simply be due to noise.

Comparable performance was obtained for the tetrameric complex ADH (148 kDa), which displayed charge states from 18+ to 24+ (Figure S5). CCS information was successfully obtained for the 20+ to 23+ charge states, yielding values ranging from 72.1 nm^2 (20+) to 74.9 nm^2 (23+). RSDs for these measurements were below 2% and consistent with previously published results.[40−42] Reported values for the 23+ charge stage of ADH range from 74.9 nm^2[41] to 69.4 nm^2[39] to 69.9 nm^2,[40] all measured based on conventional ion mobility platforms.

ADH serves as an important benchmark because it was examined in a recent study that showcased the determination of CCS values based on ion decay times measured by CDMS in an Orbitrap mass spectrometer.[43] The CCS obtained using the ion decay/CDMS method was 91 nm^2 for the 23+ charge state of ADH[43] compared to 74.9 nm^2 using the drift tube ion mobility/CDMS method in the present study. The prior study reported that accurate CCS information was difficult to obtain for complexes larger than 230 kDa because the ions survived the full length of the transient and exhibited minimal decay; the most accurate CCS values were obtained for proteins smaller than 50 kDa.[43]

Applying the drift tube-CDMS method to the tetradecameric complex GroEL (801 kDa) produced a charge state distribution from 49+ to 60+ with CCS information obtained for the 52+ to 59+ charge states (Figure S6). CCS values ranged from 193 nm^2 (52+) to 197 (59+) nm^2, with triplicate

https://doi.org/10.1021/acs.analchem.4c03379
Anal. Chem. 2025, 97, 140−146

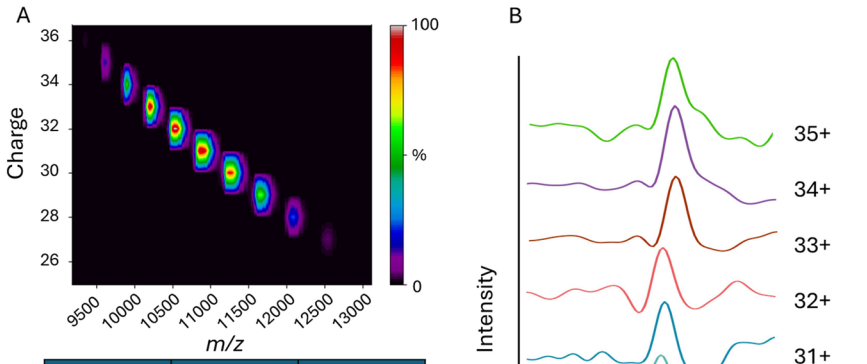

C

Charge State	Avg CCS (nm²) N = 3	CCS R.S.D (%) N = 3
35+	127	0.37
34+	127	0.20
33+	127	0.20
32+	123	0.12
31+	124	0.20
30+	123	0.28
29+	122	0.40
28+	117	0.59

Figure 5. (A) *m*/*z* versus charge heatmap for glutamate dehydrogenase. Legend denotes the relative abundance of ions. (B) Mobility spectra for the charge states analyzed by drift tube ion mobility using a drift voltage of 10 kV, step size of 3 Hz, and 15 repeats. (C) Summary of CCS values and RSDs from replicate analysis.

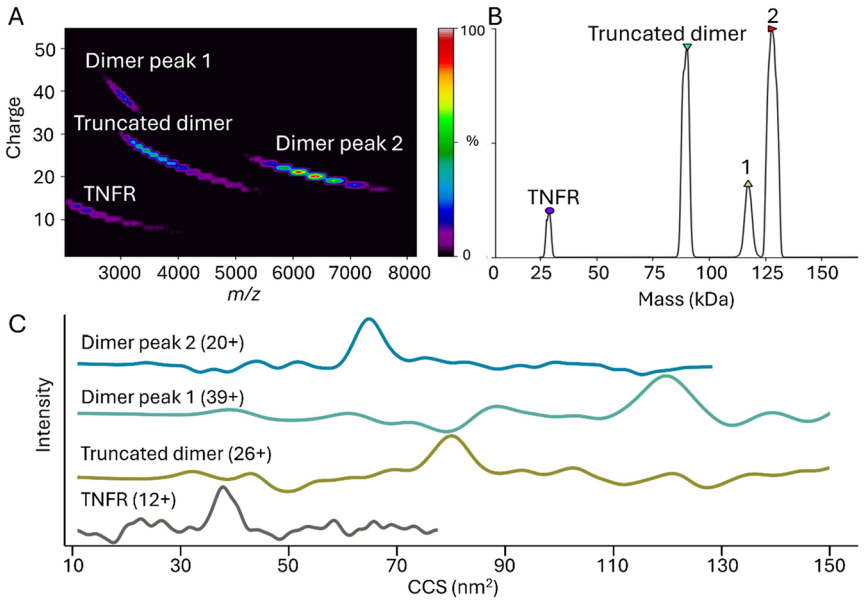

Figure 6. (A) *m*/*z* versus charge heatmap for etanercept. Legend denotes the relative abundance of ions. (B) Measured masses for the etanercept components and dimer variants from drift tube IM-CDMS experiments. (C) Mobility spectra for the charge states analyzed by drift tube ion mobility using a drift voltage of 10 kV, step size of 3 Hz, and 15 repeats.

analysis producing RSDs below 2% for all charge states. Each analyzed charge state displayed multiple features within its broader mobility spectra, features that were consistently observed in replicate experiments. Although many of these features were well resolved, baseline resolution was not achieved, likely a limitation of the drift tube. Previously reported CCS values ranged from 211 to 220 nm^2 for the 67+ charge state to 211 to 219 nm^2 for the 71+ charge state.[40−42] The notably different range of charge states for GroEL in the present study (49+ to 60+) compared to other reported studies[40−42] prevented direct comparisons of CCS values. The atmospheric pressure drift tube used here consistently results in the observation of lower charge states of proteins than observed in the absence of the drift tube,[44] possible due to charge stripping from low energy collisions as ions traverse the desolvation and mobility regions of the drift tube. These lower charge states were observed for all proteins analyzed herein. Prior attempts to measure the CCS of GroEL in the single ion regime noted that the extended survival of GroEL prevented accurate CCS calculations based on ion decay times,[45] analogous to the outcome reported in another study.[39]

The measured intact masses for all of these initial proteins analyzed were within 1% of the theoretical values, with values of 147 800 Da, 337 300 Da, and 801 000 Da for ADH, GDH,

https://doi.org/10.1021/acs.analchem.4c03379
Anal. Chem. 2025, 97, 140−146

and GroEL, respectively (Figure S7). This high degree of accuracy in intact mass measurement confirms that the drift tube CDMS method offers the ability to measure CCS values, intact masses, and charge states while also providing conformational insight.

The IM-CDMS method was then applied to the fusion protein etanercept to evaluate the feasibility of analyzing a more heterogeneous sample. Etanercept is a heavily glycosylated protein used in the treatment of several autoimmune disorders such as rheumatoid and psoriatic arthritis and consists of a tumor necrosis factor receptor (TNFR) fused to the fragment crystallizable (Fc) portion of human immunoglobulin G1 (IgG1). The protein exists as a dimer with a mass of 102.4 kDa; however due to the extensive number of glycosylation sites (6 N- and 26 O-glycosylation sites) the protein typically has an observed mass between 120 and 150 kDa.[46−48] This heterogeneity makes it an interesting target for the IM-CDMS workflow owing to the different glycoforms and protein components. To evaluate this goal, the IM-CDMS method was applied to etanercept using the same optimized parameters detailed in the previous sections.

The mass spectrum generated by CDMS revealed four distinct masses of 29.1, 90.3, 117, and 128 kDa (Figure 6). The m/z versus charge state heatmap reveals the power of CDMS in this workflow as these different species have overlapping distributions in the m/z domain; however, they are distinct in the charge domain which allows facile extraction of their individual mobility spectra. Based on the theoretical mass of the protein, the species of 29.1 kDa likely corresponds to the glycan portion of the TNFR region. Species of 90.3, 117.4, and 128 kDa correspond to different variants of the intact dimer. The species of 90.3 kDa is surprising as its mass is lower than the theoretical mass of the intact dimer; however, a previous study has shown sequence variants which are missing residues 1−186 of the TNFR region, resulting in a mass lower than the expected intact dimer.[46] The species of 128 kDa is the most abundant in the mass spectrum which aligns with the expected prevalence of glycosylation for this protein. Mobility spectra for each of these components displays CCS values that have not been readily measurable by other methods. Representative mobility spectra for the most abundant charge states of each species are shown in Figure 6C with the glycan portion of the TNFR (12+) having a measured CCS of 37.1 nm^2, the truncated dimer (26+) yielding a measured CCS of 80.1 nm^2, the 117 kDa dimer (39+) exhibiting a measured CCS of 120 nm^2, and the 128 kDa dimer (20+) demonstrating a measured CCS of 64.4 nm^2. Overall, the IM-CDMS method afforded plausible intact mass information as well as visualizing heterogeneity with respect to the sizes of the different variants of the fusion protein etanercept. This achievement provides a foundation for the analysis of heterogeneous samples not easily measured by traditional IM-MS in future studies.

CONCLUSIONS

Interfacing CDMS with ion mobility is challenging as the extended acquisition times required to generate high-quality CDMS data are incongruent with the time scale of online separation techniques. To overcome this hurdle, Fourier transform multiplexing and stepped frequency modulation were utilized to align the duty cycles of ion mobility experiments with Orbitrap-based CDMS data collection. This method was employed for analysis of the multimeric protein complexes ADH, GDH, and GroEL and provided robust and reproducible CCS data, aligning well with previously published values from conventional ion mobility studies and offering improvements in mass accuracy. The method was also applied to the glycosylated fusion protein etanercept, showcasing the ability of the workflow to analyze heterogeneous samples not readily studied by traditional IM-MS. The S/N level of IM-CDMS measurements is notably lower than conventional IM measurements, meaning that assignment of low intensity mobility features is difficult which impedes characterization of heterogeneous samples. Further enhancements to drift tube design and data processing could yield even greater resolution, paving the way for more detailed and accurate protein complex analyses and applications for structural proteomics, especially for cases which are hampered by signal or sample limitations.

ASSOCIATED CONTENT

Supporting Information

The Supporting Information is available free of charge at https://pubs.acs.org/doi/10.1021/acs.analchem.4c03379.

Additional mass spectrometer, data processing parameters, and comparison of collision cross section values obtained by CDMS to literature values and additional experimental details about calculation of collision cross sections, a charge calibration curve for standard proteins, charge distribution heatmaps, mobility spectra, and intact mass plots (PDF)

AUTHOR INFORMATION

Corresponding Author

Jennifer S. Brodbelt − *Department of Chemistry, The University of Texas at Austin, Austin, Texas 78712, United States;* orcid.org/0000-0003-3207-0217; Email: jbrodbelt@cm.utexas.edu

Authors

Kyle J. Juetten − *Department of Chemistry, The University of Texas at Austin, Austin, Texas 78712, United States*

James D. Sanders − *Department of Chemistry and Biochemistry, University of Arizona, Tucson, Arizona 85721, United States*

Michael T. Marty − *Department of Chemistry and Biochemistry, University of Arizona, Tucson, Arizona 85721, United States;* orcid.org/0000-0001-8115-1772

Complete contact information is available at: https://pubs.acs.org/10.1021/acs.analchem.4c03379

Notes

The authors declare no competing financial interest.

ACKNOWLEDGMENTS

This research was funded by NSF (Grant CHE-2203602 to J.S.B. and CHE-1845230 to M.T.M.) and the Welch Foundation (Grant F-1155). The authors thank Marielle Walti and Abigail Page for donating the GroEL plasmid and Brian Tran for producing the GroEL.

REFERENCES

(1) Mann, M.; Meng, C. K.; Fenn, J. B. *Anal. Chem.* **1989**, *61* (15), 1702−1708.
(2) Rolland, A. D.; Prell, J. S. *Chem. Rev.* **2022**, *122* (8), 7909−7951.
(3) Contino, N. C.; Jarrold, M. F. *Int. J. Mass Spectrom.* **2013**, *345*−*347*, 153−159.

(4) Todd, A. R.; Alexander, A. W.; Jarrold, M. F. *J. Am. Soc. Mass Spectrom.* **2020**, *31* (1), 146−154.
(5) Keifer, D. Z.; Shinholt, D. L.; Jarrold, M. F. *Anal. Chem.* **2015**, *87* (20), 10330−10337.
(6) Botamanenko, D. Y.; Reitenbach, D. W.; Miller, L. M.; Jarrold, M. F. *J. Am. Soc. Mass Spectrom.* **2023**, *34* (8), 1731−1740.
(7) Barnes, L. F.; Draper, B. E.; Kurian, J.; Chen, Y.-T.; Shapkina, T.; Powers, T. W.; Jarrold, M. F. *Anal. Chem.* **2023**, *95* (9), 4310−4316.
(8) Miller, L. M.; Draper, B. E.; Barnes, L. F.; Ofoegbu, P. C.; Jarrold, M. F. *Anal. Chem.* **2023**, *95* (23), 8965−8973.
(9) Barnes, L. F.; Draper, B. E.; Jarrold, M. F. *Mol. Ther. Methods Clin. Dev.* **2022**, *27*, 327−336.
(10) Harper, C. C.; Miller, Z. M.; McPartlan, M. S.; Jordan, J. S.; Pedder, R. E.; Williams, E. R. *ACS Nano* **2023**, *17* (8), 7765−7774.
(11) Harper, C. C.; Elliott, A. G.; Oltrogge, L. M.; Savage, D. F.; Williams, E. R. *Anal. Chem.* **2019**, *91* (11), 7458−7465.
(12) Kafader, J. O.; Durbin, K. R.; Melani, R. D.; Des Soye, B. J.; Schachner, L. F.; Senko, M. W.; Compton, P. D.; Kelleher, N. L. *J. Proteome Res.* **2020**, *19* (3), 1346−1350.
(13) Wörner, T. P.; Snijder, J.; Bennett, A.; Agbandje-McKenna, M.; Makarov, A. A.; Heck, A. J. R. *Nat. Methods* **2020**, *17* (4), 395−398.
(14) Du, C.; Cleary, S. P.; Kostelic, M. M.; Jones, B. J.; Kafader, J. O.; Wysocki, V. H. *Anal. Chem.* **2023**, *95*, 13889.
(15) McGee, J. P.; Melani, R. D.; Yip, P. F.; Senko, M. W.; Compton, P. D.; Kafader, J. O.; Kelleher, N. L. *Anal. Chem.* **2021**, *93* (5), 2723−2727.
(16) Kafader, J. O.; Melani, R. D.; Durbin, K. R.; Ikwuagwu, B.; Early, B. P.; Fellers, R. T.; Beu, S. C.; Zabrouskov, V.; Makarov, A. A.; Maze, J. T.; Shinholt, D. L.; Yip, P. F.; Tullman-Ercek, D.; Senko, M. W.; Compton, P. D.; Kelleher, N. L. *Nat. Methods* **2020**, *17* (4), 391−394.
(17) Wörner, T. P.; Aizikov, K.; Snijder, J.; Fort, K. L.; Makarov, A. A.; Heck, A. J. R. *Nat. Chem.* **2022**, *14* (5), 515−522.
(18) Lai, S.-H.; Tamara, S.; Heck, A. J. R. *iScience* **2021**, *24* (11), No. 103211.
(19) Wörner, T. P.; Snijder, J.; Friese, O.; Powers, T.; Heck, A. J. R. *Mol. Ther. - Methods Clin. Dev.* **2022**, *24*, 40−47.
(20) Elliott, G. A.; Harper, C. C.; Lin, H.-W.; Williams, R. E. *Analyst* **2017**, *142* (15), 2760−2769.
(21) Fuerstenau, S. D.; Benner, W. H. *Rapid Commun. Mass Spectrom.* **1995**, *9* (15), 1528−1538.
(22) Grande, A. E.; Li, X.; Miller, L. M.; Zhang, J.; Draper, B. E.; Herzog, R. W.; Xiao, W.; Jarrold, M. F. *Anal. Chem.* **2023**, *95* (29), 10864−10868.
(23) Kafader, J. O.; Beu, S. C.; Early, B. P.; Melani, R. D.; Durbin, K. R.; Zabrouskov, V.; Makarov, A. A.; Maze, J. T.; Shinholt, D. L.; Yip, P. F.; Kelleher, N. L.; Compton, P. D.; Senko, M. W. *J. Am. Soc. Mass Spectrom.* **2019**, *30* (11), 2200−2203.
(24) Strasser, L.; Füssl, F.; Morgan, T. E.; Carillo, S.; Bones, J. *Anal. Chem.* **2023**, *95* (40), 15118−15124.
(25) McGee, J. P.; Senko, M. W.; Jooß, K.; Des Soye, B. J.; Compton, P. D.; Kelleher, N. L.; Kafader, J. O. *Anal. Chem.* **2022**, *94* (48), 16543−16548.
(26) Yin, V.; Deslignière, E.; Mokiem, N.; Gazi, I.; Lood, R.; de Haas, C. J. C.; Rooijakkers, S. H. M.; Heck, A. J. R. *J. Am. Soc. Mass Spectrom.* **2024**, *35* (6), 1320−1329.
(27) Sanders, J.; Owen, O.; Tran, B.; Mosqueira, J.; Marty, M. *Anal. Chem.* **2024**, *96*, 16743−16749.
(28) Sanders, J. D.; Butalewicz, J. P.; Clowers, B. H.; Brodbelt, J. S. *Anal. Chem.* **2021**, *93* (27), 9513−9520.
(29) Butalewicz, J. P.; Sanders, J. D.; Clowers, B. H.; Brodbelt, J. S. *J. Am. Soc. Mass Spectrom.* **2023**, *34* (1), 101−108.
(30) McKenna, K. R.; Clowers, B. H.; Krishnamurthy, R.; Liotta, C. L.; Fernández, F. M. *J. Am. Soc. Mass Spectrom.* **2021**, *32* (9), 2472−2480.
(31) Reinecke, T.; Davis, A. L.; Clowers, B. H. *J. Am. Soc. Mass Spectrom.* **2019**, *30* (6), 977−986.
(32) Reinecke, T.; Naylor, C. N.; Clowers, B. H. *TrAC Trends Anal. Chem.* **2019**, *116*, 340−345.
(33) Cabrera, E. R.; Clowers, B. H. *J. Am. Soc. Mass Spectrom.* **2022**, *33* (3), 557−564.
(34) Cabrera, E. R.; Clowers, B. H. *J. Am. Soc. Mass Spectrom.* **2022**, *33* (10), 1858−1864.
(35) Grason, J. P.; Gresham, J. S.; Lorimer, G. H. *Proc. Natl. Acad. Sci. U. S. A.* **2008**, *105* (45), 17339−17344.
(36) Reinecke, T.; Clowers, B. H. *HardwareX* **2018**, *4*, No. e00030.
(37) Dodds, J. N.; Baker, E. S. *J. Am. Soc. Mass Spectrom.* **2019**, *30* (11), 2185−2195.
(38) Sanders, J. D.; Owen, O. N.; Tran, B. H.; Juetten, K. J.; Marty, M. T. *Anal. Chem.* **2024**, *96*, 15014.
(39) Kirk, A. T.; Bakes, K.; Zimmermann, S. *Int. J. Ion Mobil. Spectrom.* **2017**, *20* (3), 105−109.
(40) Bush, M. F.; Hall, Z.; Giles, K.; Hoyes, J.; Robinson, C. V.; Ruotolo, B. T. *Anal. Chem.* **2010**, *82* (22), 9557−9565.
(41) Allen, S. J.; Schwartz, A. M.; Bush, M. F. *Anal. Chem.* **2013**, *85* (24), 12055−12061.
(42) Gadkari, V. V.; Ramírez, C. R.; Vallejo, D. D.; Kurulugama, R. T.; Fjeldsted, J. C.; Ruotolo, B. T. *Anal. Chem.* **2020**, *92* (23), 15489−15496.
(43) Fisher, N. P.; McGee, J. P.; Bowen, K. P.; Goodwin, M.; Senko, M. W.; Kelleher, N. L.; Kafader, J. O. *J. Am. Soc. Mass Spectrom.* **2023**, *34* (12), 2625−2629.
(44) James, V. K.; Sanders, J. D.; Aizikov, K.; Fort, K. L.; Grinfeld, D.; Makarov, A.; Brodbelt, J. S. *Anal. Chem.* **2023**, *95* (19), 7656−7664.
(45) Bowen, K. P.; Senko, M. Determining Collision Cross Sections Using Orbitrap Charge Detection Mass Spectrometry. In *71st ASMS Conference on Mass Spectrometry and Allied Topics*, Houston, TX, June 4−8, 2023.
(46) Wohlschlager, T.; Scheffler, K.; Forstenlehner, I. C.; Skala, W.; Senn, S.; Damoc, E.; Holzmann, J.; Huber, C. G. *Nat. Commun.* **2018**, *9* (1), 1713.
(47) D'Atri, V.; Nováková, L.; Fekete, S.; Stoll, D.; Lauber, M.; Beck, A.; Guillarme, D. *Anal. Chem.* **2019**, *91* (1), 873−880.
(48) Houel, S.; Hilliard, M.; Yu, Y. Q.; McLoughlin, N.; Martin, S. M.; Rudd, P. M.; Williams, J. P.; Chen, W. *Anal. Chem.* **2014**, *86* (1), 576−584.

https://doi.org/10.1021/acs.analchem.4c03379
Anal. Chem. 2025, 97, 140−146